

# Fault Detection and Diagnosis of Industrial Robot Based on Power Consumption Modeling

Ahmad H. Sabry<sup>✉</sup>, Farah Hani Nordin, Ameer H. Sabry, and Mohd Zainal Abidin Ab Kadir, *Member, IEEE*

**Abstract**—Fault detection via power consumption monitoring of industrial robots is a substantial problem considered in this article, in which the healthy measurements of power consumption and encoders data for a prespecified task are employed as a reference for comparison to diagnose the potential failures or excessive degradation in the robot joints. Since most electrical and mechanical faults directly affect the consumed energy, the proposed solution analyzes the comparison outcomes between the healthy reference data with that monitored in a real time for each individual task. To integrate the power measurements with a base station, a ZigBee-based wireless data acquisition circuit has been developed to process the joints data. This article suggests a measurement-based mathematical model called Bode equations vector fitting as a robust fitting method to estimate such power consumption patterns. The achieved estimates allow a clear distinction for the potential failures in the robot joints that affect the power rate patterns even when involving sharp fluctuations. A table-based neural network classifier is presented to indicate the faulty joint or encoder according to the time intervals that divided for the executed task. The experimental results demonstrate the performance verification and feasibility of the proposed approach in ABB-IRB-1200 robot manipulator.

**Note to Practitioners**—Industrial machines are seeking to achieve energy optimization to verify the sustainability demand goal. Currently, many industrial robotic systems are not effectively monitored and modeled mathematically toward detecting the potential faults. In this context, a faults diagnosis method with an accurate mathematical model based on reference power patterns is proposed for monitoring the performance of that system. The proposed energy-based diagnosis technique can be readily integrated with the existent industrial robots supply and can be monitored remotely. Furthermore, no significant changes in the machine's hardware, but a reference pattern of a power consumption per each individual task per each robot, are required.

Manuscript received February 20, 2019; revised May 6, 2019 and June 11, 2019; accepted June 24, 2019. Date of publication October 14, 2019; date of current version April 30, 2020. This work was supported in part by the Institute of Power Engineering and in part by Universiti Tenaga Nasional through the UNIIG fund under Grant J510050802. (*Corresponding author: Ahmad H. Sabry*.)

A. H. Sabry, F. H. Nordin, and M. Z. Abidin Ab Kadir are with the Institute of Power Engineering, Universiti Tenaga Nasional, Kajang 43000, Malaysia (e-mail: ahmadh@uniten.edu.my; farah@uniten.edu.my; zainal@uniten.edu.my).

A. H. Sabry is with the Institute of Power Engineering, Universiti Tenaga Nasional, Kajang 43000, Malaysia, on leave from the Ministry of Electricity, Baghdad 10001, Iraq (e-mail: amr80g@gmail.com).

Color versions of one or more of the figures in this article are available online at <http://ieeexplore.ieee.org>.

Digital Object Identifier 10.1109/TIE.2019.2931511

**Index Terms**—Energy consumption, fault diagnosis, industrial robot, modeling, power patterns.

## I. INTRODUCTION

FOR industrial machines, scheduling preventive maintenance is a common procedure for improving equipment safety, maintainability, and reliability. These regulations provide a significant reduction in operational charges through dispensing of unnecessary maintenance actions and activate what is called “condition-based maintenance” (CBM) [1], which is a key tradeoff between the operational costs and maintenance. The challenge with CBM is to provide approaches that can determine the industrial machine conditions, which can be implemented by a comparison between the actual measurements/observations and the model or the reference (known behavior) for that machine. Such approaches are considered as fault indicator [2]–[4], that detect the fault existence and indicate the instantaneous status (healthy/faulty) of the equipment via the monitoring process.

In automated industries, a repeatable and continuous operation of equipment is essential to attain production requirements. Such cyclic behavior of equipment is exploited to describe a measurement-driven method of diagnoses. Considering data gathering from a cyclical operation allows detecting an abnormality by comparing the modeled with the monitored data over time of operation. Any presented approach needs to verify successful applications for diagnosing the potential failures and excessive degradations in the manufacturing robot or the mechanical faults in rotational machines. Due to only limited understandings can be embedded in a fault detection approach, it is imperative to evaluate the solutions in scenarios of real significance. The measurements-based framework allows determining mainly the parameters that affect fault detection methods, and how those parameters delimit the effectiveness of the results. Fault detection and isolation (FDI) was discussed in several studies. In [2], a parameter estimation method was considered for a permanent-magnet dc motor using block-pulse function series to estimate the motor model, or by means of error estimates of a filtered torque prediction [5].

A significant underlying in fault diagnosis is the accurate determination of a state variation. Reliable and early detection of a deformity are important to sustain service, allow sufficient time to make repairs and avoid downtime. It is also possible for measurement-driven approaches to estimate the detection of uncertainties, which support a higher level of service decisions. An industrial robot is playing the most important role and its

consumption is significant from the total energy consumption. For example, in automotive sectors, and specifically in the production phases of cars, the consumed energy by the robots is about 8% of entire consumption [6]. For that reason, it is important to analyze the characteristics of the consumption rate and modeling the power consumption pattern of industrial robots to make possible energy efficiency optimizations.

In recent times, many studies have been published on the analysis and modeling of energy consumption in industrial robots [6]–[13]. Commonly, there are a variety of components in robotic systems that consume energy, for instance, controllers, fans for the cooling, motors, and the joint's friction of the robot. In [7], the motor characteristics were analyzed by modeling the energy consumption of the ABB IRB 1200 robot based on a method of parameters identification from the power data rather than joint torque.

In [8], the authors suggested a configuration scheme of an energy-efficient robot for industrial application. Both studies [9] and [13] analyzed the characteristics of the delivered electricity for an industrial robot to compare their energy consumptions in various operation conditions, for instance, different trajectories, tool weights, different work-piece positions, and at various speeds. In [6], authors proposed detailed modeling of energy consumption for an industrial robot that includes the converters consumption, inverters, dc bus, electromechanical brakes, and motors, but their model requires more parameters, several of them are secret and inflexible to obtain. Pelliciari *et al.* [11] offered a model for the consumption of industrial robot energy while calculated the trajectories of optimal energy by means of constant-time scaling, with the assumption of the inertial parameters being already known for the robot. Paryanto *et al.* [12] employed Modelica-based simulation tools to produce digital modeling of a six-axis industrial robot based on experimental measurements to improve the modeling precision, where the effects on the robot parameters, such as payload and speed, were also analyzed in terms of energy consumption. One study addresses the monitoring of industrial robot but in terms of its trajectory and path planning using Android device and Wi-Fi communication [14].

For modeling the power consumption rate of industrial robots, a robot's dynamics is essential to explore. Since the losses due to inertia and frictions are confidential and unknown for users, many studies addressed these issues by adopting parameter identification techniques [15]–[20]. Some researches discussed Denavit–Hartenberg notation when identifying the parameters of the industrial robot consumptions which is employed to identify the kinematic coefficients and to indicate the frames of robot joint, the results of that notation is vital on computing the dynamic and kinematic system parameters which is based on end-effector position [21], [22].

Although those efforts utilize the parameter identification toward modeling the power consumption, more attention needs to be explored, such as torque–speed relations with respect to actuator consumption that are usually required for the profile modeling and identifying the influence of robot parameters on consumption.

Commonly, the fault diagnosis uses residual signatures to create a fault indicator, which depends on the deviations between the model/reference of a system and its measurements. A model of a particular system is a mapping of input–output data, which delivers essential information about system behavior that is important for fault diagnosis system. There are several methods to create the data residuals such as the observations/measurements, and parameter identifications. Therefore, alternatives are still available at costly system modeling. Some alternatives require additional knowledge about system observations or more sensory information. Although with those above research, that employed efficient techniques for modeling the energy consumption and lead rising in energy system efficiency of industrial robot systems, they did not offer an accurate model describing that power consumption.

The electrical power of robot joints can be measured suitably by means of power sensors that can be used to estimate consumption of a particular task, but due to the lack of power sensors and their accessibility, this article presents a strategy of adopting a measurement-driven method to model the power consumption of a robot manipulator. A data acquisition card [23] with a high sampling time is developed to acquire the measurements of fault-free power consumption per each individual task to be recorded as a reference pattern of that task. The procedure includes approximating the consumption data by a model called Bode equations vector fitting (BEVF) as an accurate alternative of the modeling by parameters identification [24]. BEVF model is employed as a robust algorithm to estimate such power profiles that have complex variation and many resonance peaks. The modeled/reference data of a fault-free power pattern and encoders data for a prespecified task are employed as a reference for comparison to diagnose potential failures in the joints, where here is implemented on ABB-IRB-1200 robot manipulator.

The objective of this article is to formulate a methodology addressing detection and isolation problems of realistic failures that might take place in a robot manipulator running in an industrial environment (e.g., pick and place, assembly, and polishing tasks in products manufacturing). Particularly, this article focuses on the power consumption profiles and their relation with a fault signature in manipulator's joints exploiting the available position-sensors connector of the user. Therefore, seeking of fault signature is driven by engineering insight and experience that allows correlating power profile behaviors with various types of physical failures, in a manner that makes the implementation of FDI procedure cost effective and easy to use by operators.

#### A. Dynamic Power Model of a One Joint

Since this research focuses on the net energy consumption of robot actuators, an experiment has been conducted on a single actuator to measure the power consumed delivered by a dc power supply. Therefore, it produces two types of losses: the main electrical power losses due to the actuator mechanical and electrical elements, and the power consumptions due for controlling speed and position of a link. A standby or idle power

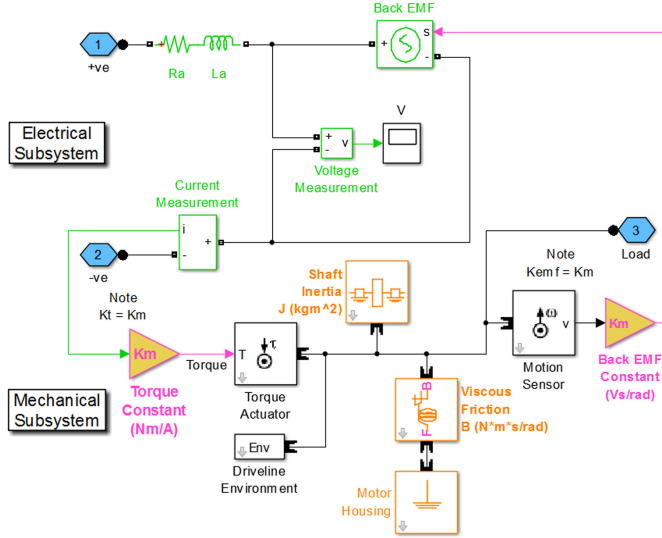


Fig. 1. DC servomotor modeling.

is sometimes provided by a manufacturer with respect to the terminal voltage ( $P_{\text{stby}}$ ); these losses are significant in low-power states.

Thus, the drawn power from a power source  $P_s$  can be given by

$$P_s = \mu_c \cdot P_e + P_{\text{stby}} \quad (1)$$

where  $\mu_c$  is the controller efficiency. The electrical energy  $E_{\text{elec}}$  of a power source is calculated by the integration power over time

$$E_{\text{elec}} = \int P_s(t) dt. \quad (2)$$

Unfortunately, the electrical and mechanical parameters of robot motors are not provided in its datasheet. Therefore, an optimization algorithm is used to estimate these parameters; MATLAB-based nonlinear least-square technique is employed to tune servomotor parameters toward the actual values depending on input–output experimental measurements [25]. A dc servomotor using first principles, with its electrical and mechanical components, can be represented as shown in Fig. 1.

The motor model illustrates current ( $I$ ), torque ( $\tau_m$ ), and motor speed ( $\omega$ ) to the back electromotive force (EMF) ( $e$ ) relationships; it also includes the electrical parameters (armature inductance ( $L_a$ ) and resistance ( $R_a$ )) and the mechanical parameters (shaft inertia, viscous friction (damping)). The value of the current interprets the consumed power of a motor. Therefore, we derive, in this section, the model equation of the current by considering the dc servomotor dynamic model.

Using Kirchhoff's voltage, a differential equation for the equivalent circuit can be written by

$$V = L_a \frac{dI}{dt} + R_a I + k_b \omega \quad (3)$$

where  $k_b$  denotes the motor voltage constant which is determined by the reluctance of the iron core, number of turns of the armature winding, and the flux density.

From a mechanical perspective, performing an energy balance on the system requires that the summation of the torques on the motor must equal zero. Thus

$$\tau = J_m \frac{d\omega}{dt} + \tau_m \quad (4)$$

where  $\tau$ ,  $J_m \frac{d\omega}{dt}$ , and  $\tau_m$  denote the torques: of motor electromagnetic, of the velocity of the rotor, and of the mechanical load, respectively.  $J_m$  represents the inertia of the equivalent mechanical load.

The armature current ( $I$ ) is proportional to the electromagnetic torque  $\tau$  and can be given by

$$I = \frac{\tau}{k_b} = \frac{J_m \frac{d\omega}{dt} + \tau_m}{k_b} = \frac{\tau_m}{k_b} + \frac{J_m}{k_b} \cdot \frac{d\omega}{dt}. \quad (5)$$

Therefore, the variation rate in motor current is given by

$$\frac{dI}{dt} = \frac{1}{k_b} \cdot \frac{d\tau}{dt} = \frac{1}{k_b} \frac{d\tau_m}{dt} + \frac{J_m}{k_b} \cdot \frac{d^2\omega}{dt^2}. \quad (6)$$

Thus, substituting (5) and (6) in the motor terminal voltage (3) results in

$$V = \frac{L_a}{k_b} \cdot \frac{d\tau_m}{dt} + \frac{L_a J_m}{k_b} \cdot \frac{d^2\omega}{dt^2} + \frac{R_a}{k_b} \cdot \tau_m + \frac{R_a J_m}{k_b} \cdot \frac{d\omega}{dt} + k_b \omega. \quad (7)$$

Thus, the second derivative of the angular speed is

$$\begin{aligned} \frac{d^2\omega}{dt^2} &= \frac{k_b}{L_a J_m} V - \frac{1}{J_m} \cdot \frac{d\tau_m}{dt} - \frac{R_a}{L_a J_m} \cdot \tau_m \\ &\quad - \frac{R_a}{L_a} \cdot \frac{d\omega}{dt} - \frac{k_b^2}{L_a J_m} \cdot \omega. \end{aligned} \quad (8)$$

To simplify the solution, we suppose that the mechanical load ( $\tau_m$ ) is constant, which means that only motor under the test is activated at the test time ( $\frac{1}{J_m} \cdot \frac{d\tau_m}{dt} = 0$ ).

From (3), the angular speed and current rate are given by

$$\frac{d\omega}{dt} = \frac{\tau - \tau_m}{J_m} \quad (9)$$

$$\frac{dI}{dt} = \frac{V}{L_a} - \frac{R_a}{L_a} I - \frac{k_b}{L_a} \omega. \quad (10)$$

Equations (8)–(10) can be written in a state-space form as

$$\begin{bmatrix} d^2\omega/dt^2 \\ d\omega/dt \\ dI/dt \end{bmatrix} = \begin{bmatrix} -\frac{R_a}{L_a} - \frac{k_b^2}{L_a J_m} & 0 \\ 1 & 0 \\ 0 & -\frac{k_b}{L_a} - \frac{R_a}{L_a} \end{bmatrix} \begin{bmatrix} d\omega/dt \\ \omega \\ I \end{bmatrix} + \begin{bmatrix} \frac{k_b}{L_a J_m} V - \frac{R_a}{L_a J_m} \cdot \tau_m \\ 0 \\ \frac{V}{L_a} \end{bmatrix}.$$

To solve these differential equations, the initialization of the motor parameters was extracted. Then, integration of the above equations is achieved by using MATLAB functions `ode23` and `ode45`. The transient process for three states, speed derivative ( $d\omega/dt$ ), rotational speed ( $\omega$ ), and the motor current ( $I$ ), are shown in Fig. 2.

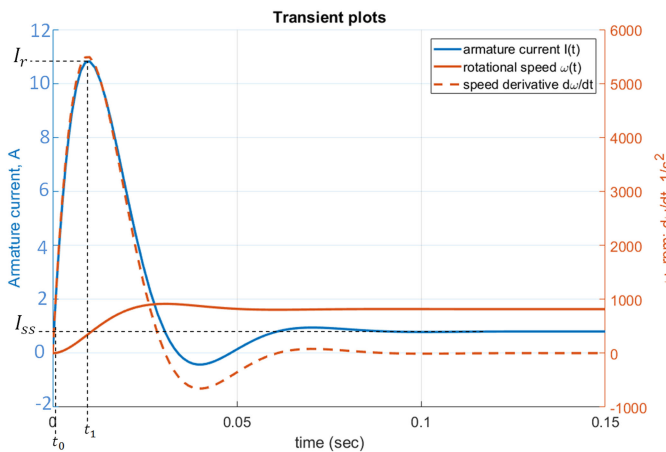


**Fig. 2.** Transient process for the three states; speed derivative ( $d\omega/dt$ ), rotational speed ( $\omega$ ), and the motor current ( $I$ ).

The motor armature current approaches the value ( $I_r = \frac{V}{R_a}$ ) exponentially due to the existence of an inductance represented by the factor ( $L_a \neq 0$ ) in the armature circuit, which can be given by

$$I(t) = I_r \left(1 - e^{-\frac{t}{T_a}}\right) \quad (11)$$

where  $T_a = L_a/R_a$  is the motor electrical time constant. The current  $I(t)$ , corresponding to the load torque  $\tau_m$ , reaches the value  $I_{ss} = \tau_m/k_b$  at the time instant  $t = t_0$ , on which the motor starts rotating and EMF ( $e = k_b\omega$ ) is induced on its windings. The armature current continues rising until  $t = t_1$ , at which the angular acceleration ( $\frac{d\omega}{dt} = \frac{\tau - \tau_m}{J_m}$ ) reaches its maximal, then  $I(t)$  gradient to the  $I_{ss}$  value and the angular speed move toward a value of the steady state.

To show the influence of some electrical and mechanical factors on the consumption transient, three values (its value, half and double) for each discussed parameter are simulated and compared. Fig. 3(a) displays the variation of the armature resistance, where the starting value of the armature current has reduced due to increase in the armature winding resistance; however, its steady-state value remains with no change as it relies on mechanical load. Fig. 3(b) displays the variation of the armature inductance, where an increase in the armature inductance increases the armature current and the electromagnetic torque and added more oscillation on the transient process, but the starting inrush value of the armature current has reduced with no change in its steady-state value. Fig. 3(c) displays the variation of the armature inertia, where the electromechanical time constant increases due to an increase of the armature inertia, the electromagnetic torque, and the armature current decreases result in a periodic transient. Although the steady-state value of the current does not change, the inrush current over startup time increases due to an increase in the moment of inertia. Increasing of armature inertia usually means an increase in the rotor mass or additional mechanical load on the motor shaft. Fig. 3(d) displays a variation of the magnetic flux, where the transient operation profile and the current steady state are significantly

influenced by the difference in the magnetic flux of the motor. The inrush current during startup decreases and its steady-state value decreases at a constant load torque. Fig. 3(e) displays the variation of supply voltage on the consumption transient, where the starting motor current increases according to the increase in the applied voltage.

### B. System Modeling and Faults

In order to choose the diagnosis solution, it is important to understand the behavior of the system and its influence by the faults. This can be achieved with the use of models. A system model describes the relationships between variables affecting the system. Therefore, if we consider the measurements of the power consumption  $P(t)$ , the relation can be formulated as

$$P(t) = f(c, v, t)$$

where the power consumption is a function of different parameters represented by  $c$ , which is a vector of constant parameters such as the surrounding conditions and the task, while  $v$  and  $t$  denote the variables vector and the time, respectively. Modeling can be performed based on first principles, e.g., from the laws of physics, where the parameters of the resulting model will have some physical meaning. In case there are parameters with unknown values, these can be determined empirically, e.g., from an identification procedure. An alternative to modeling from first principles is to choose the model based on how well it describes the data, where the parameters have no obvious physical interpretation. To calculate energy consumption, two models have been considered for comparison purposes. The first is the mechanical one of the robot which is given by

$$E_{\text{mech}} = \int_{t_0}^{t_1} |v \cdot F| dt \quad (12)$$

where  $v$  and  $F$  denote the robot end-effector velocity and vector of total forces, respectively, and  $t_0$  and  $t_1$  denote the start and end times of a task ( $t_1 - t_0$ ). For dc motor-driven robot, we will compare (1) with the total electrical energy consumed by the motors as follows:

$$E_{\text{elec}} = \sum_i \left( \int_{t_0}^{t_1} |\tau_i \cdot \omega_i| dt + \int_{t_0}^{t_1} R_i I_i^2 dt \right). \quad (13)$$

$\tau$  and  $\omega$  denote the motor torque and angular velocity, respectively.  $I$  denotes the current calculated by ( $I = \tau/r \cdot K_\tau$ ), where  $r$  denotes the servomotor gear ratio, and  $K_\tau$  is the torque constant. The power losses are represented by the second term of the  $E_{\text{elec}}$  equation ( $R_i I_i^2$ ). However, one study [7] took the efficiency  $\mu_i$  of the motor in consideration when modeling the energy consumption of such a system, which is given by

$$\begin{aligned} E_{\text{elec}} &= \sum_i \frac{\left( \int_{t_0}^{t_1} |\tau_i \cdot \omega_i| dt + \int_{t_0}^{t_1} R_i I_i^2 dt \right)}{\mu_i} \\ &= \sum_i \frac{\left( \int_{t_0}^{t_1} P_{t,i} dt \right)}{\mu_i} \end{aligned} \quad (14)$$

where  $i = 1, 2, 3, \dots, n$  which is the number of degree of freedom, while  $P_{t,i}$  denote the total power consumption at the

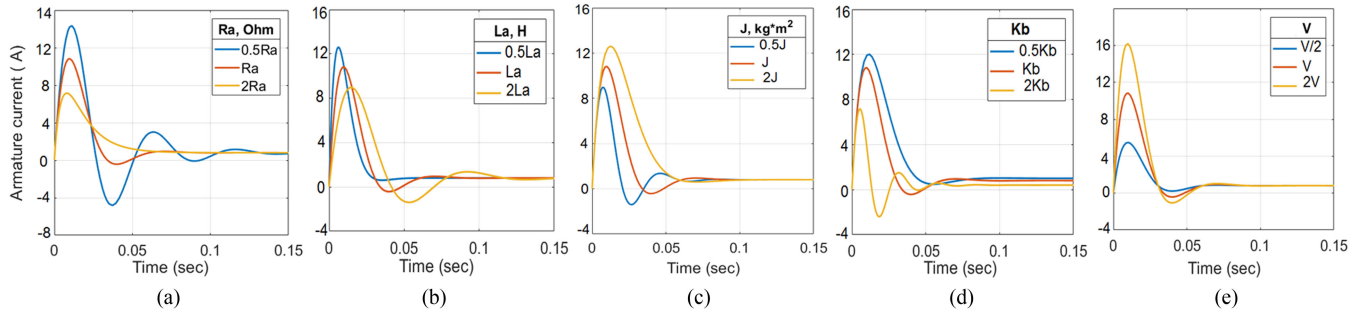


**Fig. 3.** Influence on consumption transient of (a) armature resistance, (b) armature inductance, (c) armature inertia, (d) magnetic flux, and (e) supply voltage.

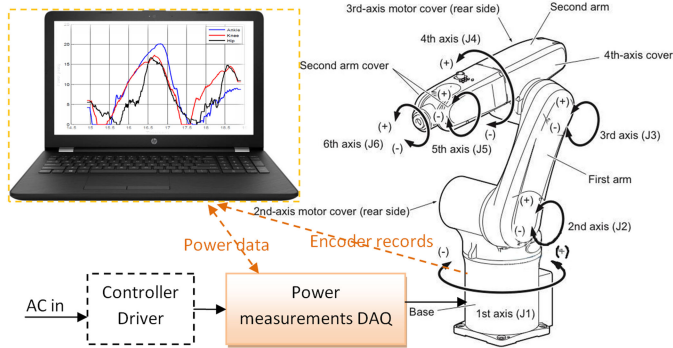


**Fig. 4.** Experimental setup of the proposed method.

ith joint. The entire power consumption of the industrial robot is composed of the consumption due to a control system and the portion due to the auxiliary components ( $P_a$ ).  $P_a$  includes the power consumption for an air compressor of the pneumatic mechanism, cooling fans, and the computer PC as a control and monitoring station. Auxiliary components consumption is usually constant [7], [26]. The control system power comprises the losses due to ac–dc converters, dc bus, inverters, etc., and the power supply of driving the robot motors.

Based on the measurements experience, the power consumption of a particular multidegree industrial robotic arm for a specified task, speed, load, and the surrounding temperature is unique. Consequently, the electric power consumption pattern is considered as a signature under those parameters. Only the temperature of the operating environment has assumed as a constant during the measurements and tests in this work. Therefore, we can write the power consumption as a function of these parameters as follows:

$$E_{\text{elec}} \text{ or } P_t = f(\text{task, speed, load, } T, t) \quad (15)$$

where  $T$  and  $t$  denote the temperature and the time, respectively.

## II. ENERGY CONSUMPTION MODELING

To describe the proposed procedure, this article employs the ABB IRB industrial robotic arm, where its joints are actuated with a brushless motor which includes an encoder to measure its position. The experimental setup can be described as in Fig. 4,

while the overall flowchart of the proposed methodology is shown in Fig. 5.

## III. BEVF MODELING

BEVF technique is a measurement-based algorithm utilizing the numerical fitting robustness of the vector fitting (VF) method [27], which is employed in this article to model power consumption patterns of the multidegree robot. However, the BEVF algorithm is composed of three stages: input adaptor, VF process, and output adaptor stages to produce the system's mathematical equations. BEVF algorithm can be demonstrated as in Fig. 6, where  $P_1(t)$ ,  $P_2(t)$  are the two mathematical expression options of the power consumption rate,  $n$  is the order of the modeling equation, and  $r_k$ ,  $p_k$ , and  $K$  are the equation's coefficients and they could be real or complex numbers. These coefficients could be complex numbers; therefore,  $\text{im}(x)$  and  $\text{re}(x)$  denote the imaginary and the real parts of the variable  $x$ , respectively.

## IV. FDI CRITERIA

We assume that there is no fault that can be detected for a joint at rest, and it is supposed that any variation in power consumption reflects a drift in the encoder records.

In this article,  $q_{ri}(t)$  denotes the required/reference position of the  $i$ th joint at time  $t$ , while  $q_{mi}(t)$  denotes the measured value from the corresponding position sensor. There is an accessible encoder/resolver per each joint that provides a measure for the position at time  $t$  and a measure of the total power consumption for the robot manipulator  $P_{mi}(t)$ , which compares with the reference one  $P_{ri}(t)$ . For the fault-free case

$$\begin{aligned} |q_{ri}(t) - q_{mi}(t)| &< \epsilon_q \\ |P_{ri}(t) - P_{mi}(t)| &< \epsilon_p \end{aligned} \quad (16)$$

where  $\epsilon_q$ ,  $\epsilon_p$  denote the tolerance in position and power consumption, respectively. If (16) is false, this indicates a disagreement between the encoder and the power consumption measurement; this is due either to a fault in the encoder or the other joint components. In order to distinguish the faults between the position sensor and corresponding joint components, we adopt two criteria for isolating the fault:

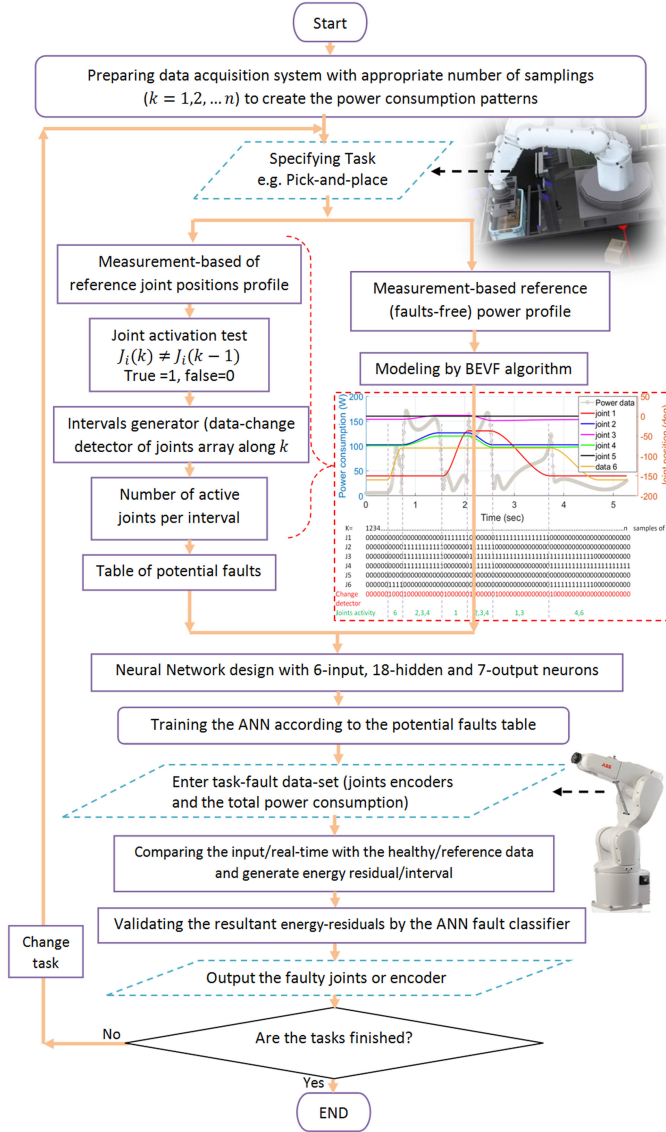


Fig. 5. Methodology diagram.

- 1) If  $|P_{ri}(t) - P_{mi}(t)| < \epsilon_p$  and  $|q_{ri}(t) - q_{mi}(t)| > \epsilon_p$ , then the fault on the  $i$ th encoder is indicated, which means that the encoder has a constant measure that does not match the measurement of the reference position obtained from the historical data.
- 2) If  $|P_{ri}(t) - P_{mi}(t)| > \epsilon_p$  and  $|q_{ri}(t) - q_{mi}(t)| > \epsilon_p$ , then a failure in joint components is indicated but with two possibilities: indicates a faulty encoder as well, or healthy but merely reflects the joint failure.

## V. RESULTS OF A MANUFACTURING TASK

An industrial robot of six-degrees of freedom (6-DoF) ABB IRB is employed to demonstrate the proposed modeling of energy consumption based on power rate measurements. The stroke, reach, working range, load, and the robot's frame assignments are shown in Fig. 7.

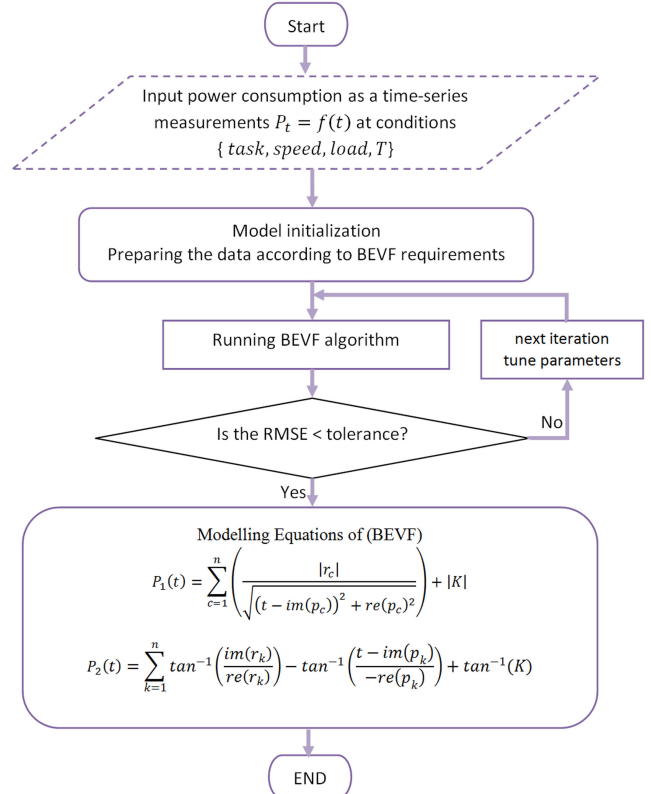


Fig. 6. BEVF implementation diagram.

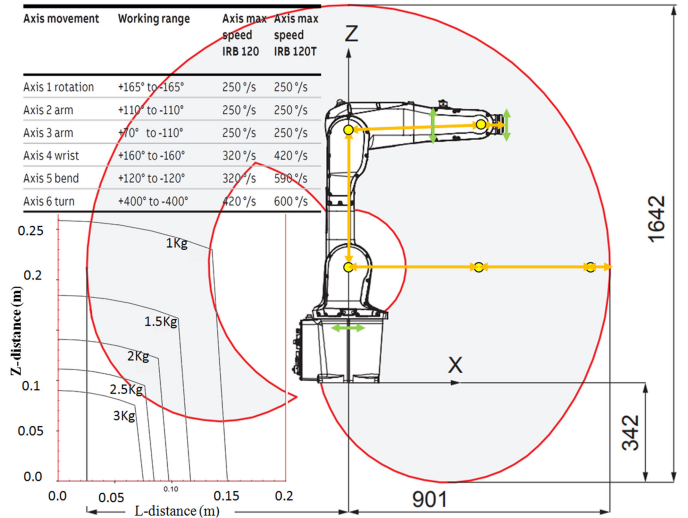
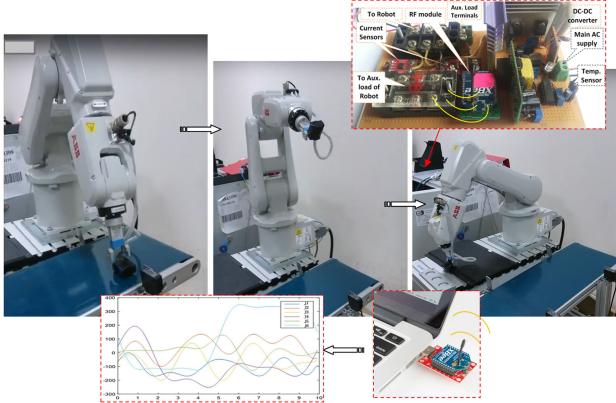
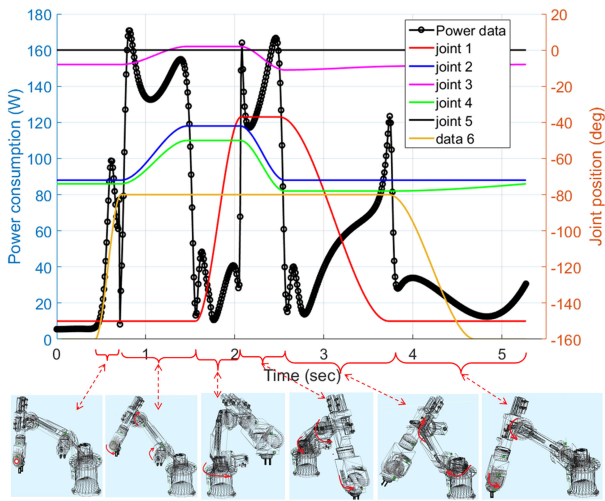


Fig. 7. Stroke, reach, working range and load for ABB-IRB-1200 robot.

Basically, the accuracy of the measurements affects the accuracy of energy consumption modeling. Current and voltage sensors were utilized to record the data at an appropriate sampling time reach to the 123 Hz maximum for the employed circuit. The procedure uses wireless ZigBee-based monitoring circuit for recording the energy parameter measurements [23]. The experimental setup diagram for the power consumption measurements with the data acquisition board is shown in Fig. 8.



**Fig. 8.** Experimental setup diagram of the consumption measurements system.



**Fig. 9.** Experimental measurements of the power consumption rate of ABB IRB1200 industrial robot when performing a pick-and-place task.

Experimental measurements have been conducted to inspect the impact of mechanical factors, such as the wear in robot joints and unexpected obstacles, and electrical factors such as the faults of the speed controller or the drift in armature circuit parameters on the energy consumption under a specified speed of a manufacturing task.

#### A. Pick-and-Place Task

A pick-and-place task has been conducted in which its end-effector installed with a gripper tool catching a load in the half of the full task trajectory to release the load again and so on. The robot task has been configured so that its end-effector speed has set to a constant value equal to 0.3 rad/s, 200 g load, and 28 °C. The acquired experimental measurements of both power consumption and the joints encoders according to the proposed time intervals are shown in Fig. 9.

As per the proposed algorithm described in Fig. 5, the power pattern has been divided into intervals according to any change in the joints under excitation based on data change in the corresponding encoders. This is performed by a data change detector and for each new task, which needs to be recorded and stored

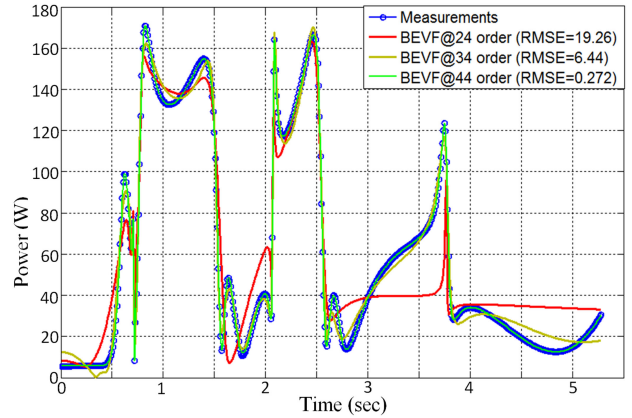


**Fig. 10.** Power data modeling till the 12th iteration,  $N = 24, 34$ , and  $44$  orders of approximation.

as a reference for these patterns under healthy conditions. The red color arrows on the robot images indicate the exciting joints to move during that interval, while those underneath the x-axis indicate the stage period from one side and its associated robot movement from another side. The peaks that have observed in the power consumption rate measurements specifically at  $t = \{0.74, 1.52, 2.17, 2.6, 3.73\}$  s, at the deceleration and acceleration stages, are due to the fast changes in the joint friction torque when varies from maximum asperity to minimum or vice versa when the velocity changes over. Higher energy consumed when a number of exciting joints contribute to performing that part of end-effector moving with its load, which can be observed at the second and the fourth periods. This result represents the required data for modeling that would use as a reference for this specified task.

**1) Modeling the Power Measurements by BEVF:** Several attempts have been performed with different adjustments for BEVF parameters to tune the approximation, such as the order of approximation ( $N$ ), iterations, and distribution of model poles according to the resonance peaks of the power pattern. However, in brief, three modeling are presented under different conditions; the first has 24th order of approximation with root mean square (rms) error of 19.26, the second has 34th order of approximation with rms error of 6.44, and the third with a very clear agreement between the measurements and the model data, which was obtained at the 44th order of approximation with rms error = 0.2715. All these models were performed until the 12th iteration and are shown in Fig. 10.

As described in [28], the mathematical formulas of the BEVF modeling are generalized as

$$P_1(t) = \sum_{k=1}^n \left( \frac{|r_k|}{\sqrt{(t - \text{im}(p_k))^2 + (\text{re}(p_k))^2}} \right) + |K| \quad (17)$$

$$P_2(t) = \sum_{k=1}^n \tan^{-1} \left( \frac{\text{im}(r_k)}{\text{re}(r_k)} \right) - \tan^{-1} \left( \frac{t - \text{im}(p_k)}{-\text{re}(p_k)} \right) + \tan^{-1}(K). \quad (18)$$

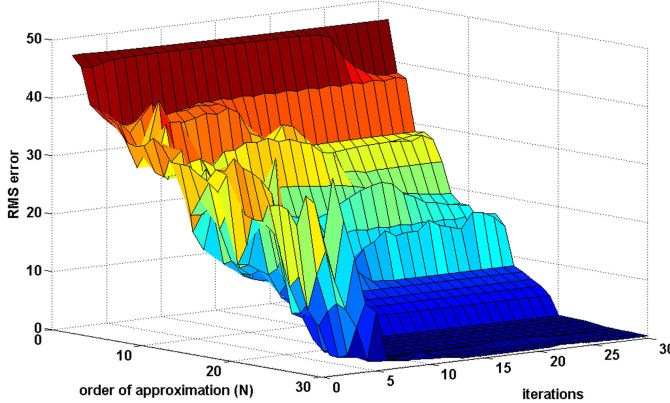


**Fig. 11.** RMS error along with: order of approximation ( $N$ ) and iterations.

In this article, the first formulating expression, given by (17), is considered as an initialization process of this algorithm. Therefore, the coefficients of the power model  $P_1(t)$  for the above 34th and 44th-order models were extracted and listed in Appendix A.

**2) Fitting Evaluation:** The RMS error has been considered to measure the model performance for data approximation, which is given by

$$\text{rms error} = \sqrt{\frac{1}{n} \sum_{i=1}^n (p_i - p_{ei})^2} \quad (19)$$

where  $p_i$  denotes power measurements and  $p_{ei}$  denotes model/estimates. The performance evaluation of the developed modeling can be expressed as shown in Fig. 11.

According to the results in the above 3-D graph, the rms error decreases with the increase in the order of approximation and the number of iterations. Although the accuracy and adequacy of the developed modeling improving with the rise in the resultant order and iteration, higher order reveals higher complexity in the created mathematical equation. It is observed that 10–20 iterations are sufficient to obtain reasonable convergence.

To highlight the significance of the proposed fitting model, several fitting equations have been applied for modeling the measurements of the same power pattern. However, only equations with reasonable fitting have been considered such as; 8th order of Gaussian, 8th order of Fourier, 8th order of sum of sine, and the 9th order of a polynomial, as shown in Fig. 12.

The aforementioned orders of the fitting models are the maximum offered by MATLAB [29]. It can be observed that all the above models do not match as well with the experimental results as in the BEVF model, where the figure's legend indicates the rms error of each individual model with respect to the measurements.

### B. Fault Diagnosis

**1) Scenario 1: Pick-and-Place Task:** To study the action of mechanical and electrical faults on the power consumption pattern, a spring is fixed on one joint which is excited in four stages of pick-and-place task. An extension spring of about

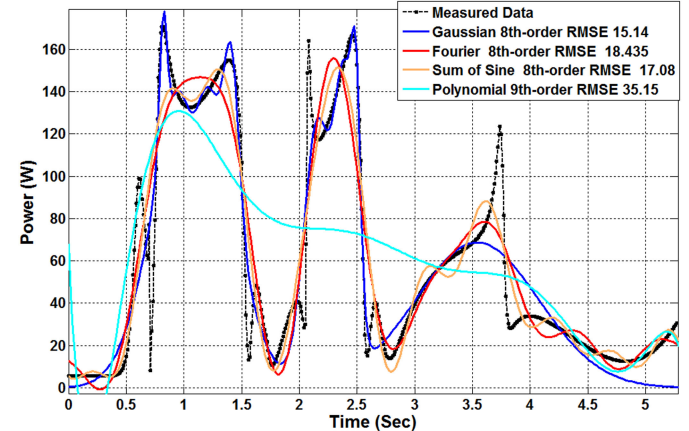


**Fig. 12.** Comparison of different fitting models and their rms error values.

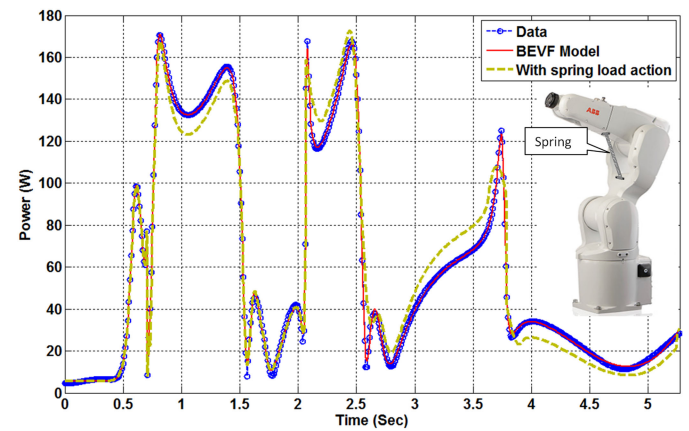


**Fig. 13.** Comparison of the reference/model with under-spring action.

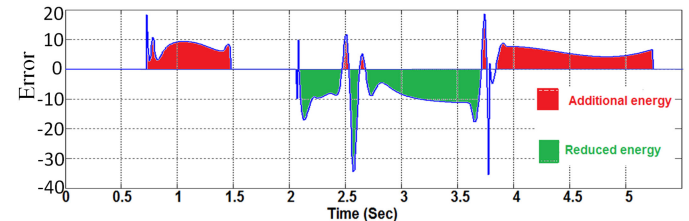


**Fig. 14.** Energy difference between reference/model with under-spring action.

300 mm length and 10 N maximum was fixed to obstruct the rotation of the elbow joint. The measurements have been conducted under the same conditions as that for healthy experiment and recorded on one graph with the previous data as shown in Fig. 13, while the error difference between the measurements under spring load action and the references is shown in Fig. 14.

Referring to Figs. 13 and 14, the result shows a clear agreement over some time intervals and disagreements elsewhere between the reference (healthy or model) data and that under the spring load. It is noted that additional energy generated when a rotational motion opposite the gravitational force of

**TABLE I**  
ASSIGNING FAULTY JOINT ACCORDING TO ACTIVATED TIME INTERVAL

Time interval	joint No.					
	1	2	3	4	5	6
First	0	0	0	0	0	-1
Second	0	0	1	-1	1	-1
Third	1	-1	0	0	0	0
Fourth	0	0	1	-1	1	-1
Fifth	1	-1	0	0	1	-1
Sixth	0	0	0	1	-1	1
Target	Y1	Y2	Y3	Y4	Y5	Y6
	1	-1	1	-1	1	-1

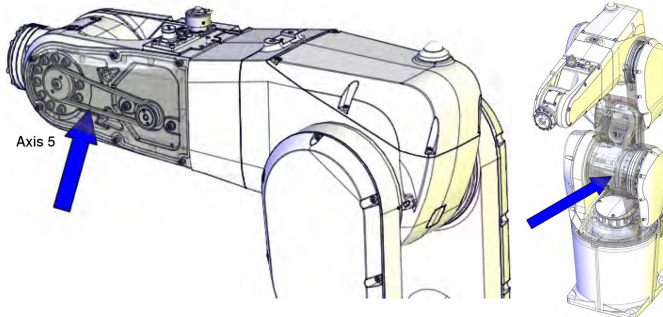


Fig. 15. Location of the belt in axis 5 and the controller of axis 2.

end-effector, and conversely, a reduction in energy occurs in the interval that joint moves toward the ground in line with gravitation. The mechanical load has impeded the elbow joint rotation and effects on the consumed energy; this power either added as additional power consumption as indicated in the interval  $\{2.1\text{--}3.7\}$  s or a reduction as in the intervals  $\{0.7\text{--}1.5\}$ , and  $\{3.5\text{--}5.4\}$  s. These changes in power pattern reflect the effect of obstacles on power consumption and can help to indicate joint components that have a problem. Based on the above description, it can be prepared a table of fault diagnosis according to the divided intervals of this task to indicate which joint suffering from problem accordingly as indicated in Table I.

It is clear that a fault in any joint of the manipulator will produce a change in the consumed energy. When energy residual exceeds a preset threshold of particular intervals, a fault is detected at once.

**2) Scenario 2: Polishing Task, Two Faulty Joints:** To evaluate the effectiveness of the proposed algorithm in a multi-faults, another scenario is performed. A polishing task is tested by setting two faults, electrical by removing the driving signal from joint 2, and mechanical by removing the belt of joint 5, as may be shown in Fig. 15. The task performing stages and the power patterns under both healthy and faulty conditions are shown in Fig. 16.

Measurements have been acquired from the monitoring circuit of this scenario for the joints encoders and the net power consumption under two conditions; faults-free (reference) data, and the faulty (two faulty joints) data, as demonstrated in Fig. 17.

Referring to Figs. 16 and 17, the data change detector of encoders under healthy/reference conditions indicate ten intervals for this scenario; three intervals display a change in the

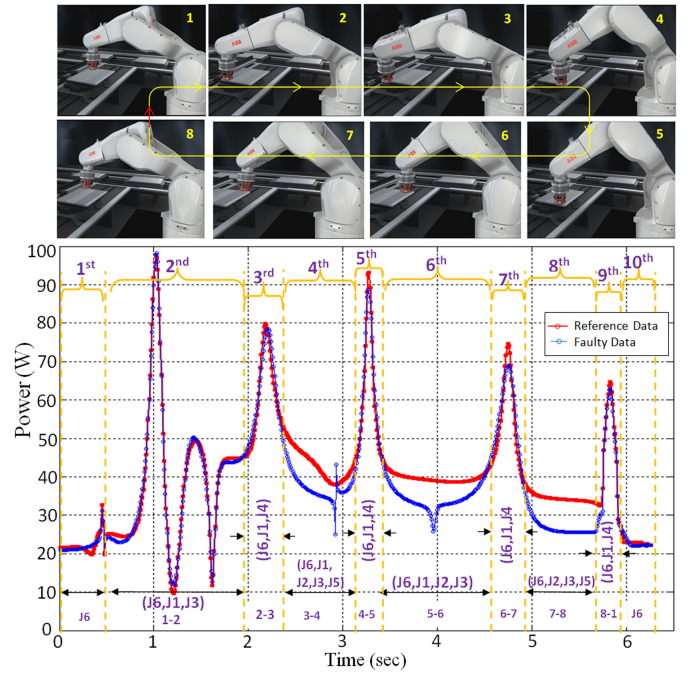


Fig. 16. Performing stages of polishing task, and the power patterns under both healthy and two-joint faulty conditions.

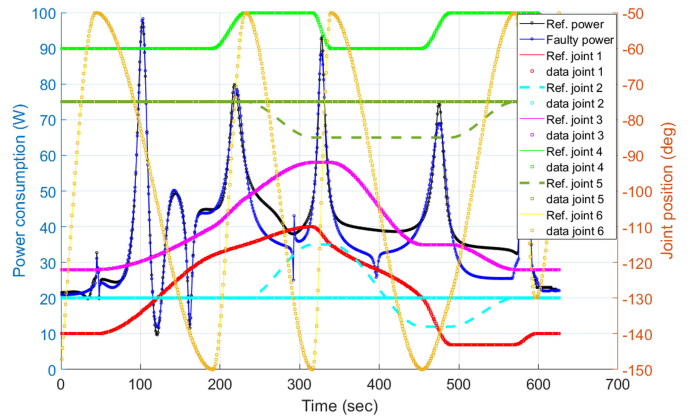


Fig. 17. Two faulty joints (joint 2 and joint 5) with their encoders.

power profile. The faulty measurements in Fig. 17 also show the agreement between encoders and consumption profile (blue color), where both joint 5 and joint 2 stay with no change with respect to their references. This also provides evidence that the corresponding joints have a problem.

**3) Scenario 3: Polishing Task, Two Faulty Joints, and One Faulty Encoder:** Referring to Fig. 18, an experiment of the same faults conditions for Scenario 2 was performed but with partial change with respect to healthy/reference conditions. This measurement shows agreement between the encoder of joint 5 with the faulty consumption profile (blue color) in the faulty intervals, while disagreement in the case of the encoder of joint 2, where only small change occurs during the faulty intervals.

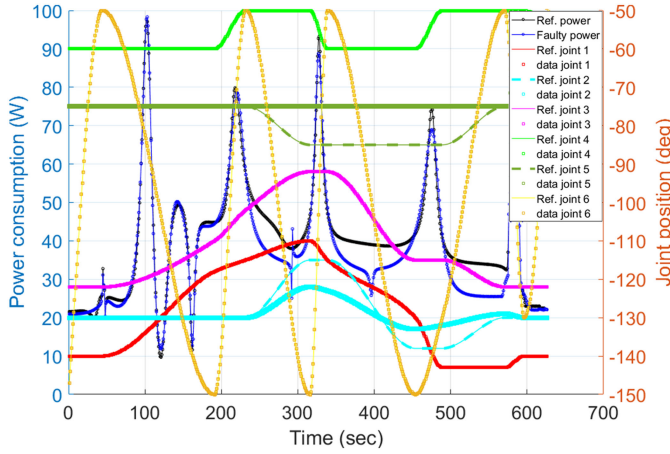


Fig. 18. Two faulty joints (joint 2 and joint 5) and one encoder of joint 2.

TABLE II  
FAULTS TABLE OF THE POLISHING TASK

Time interval	joint No.					
	1	2	3	4	5	6
First	0	0	0	0	0	0
Second	1	-1	0	0	1	-1
Third	1	-1	0	0	0	1
Fourth	1	-1	1	-1	0	0
Fifth	1	-1	0	0	0	1
Sixth	1	-1	1	-1	0	0
Seventh	1	-1	0	0	0	1
Eighth	0	0	1	-1	0	0
Ninth	1	-1	0	0	0	1
Tenth	0	0	0	0	0	0
Target	Y1	Y2	Y3	Y4	Y5	Y6
	1	-1	1	-1	1	-1

Now for the polishing task, it can also be prepared a table of fault diagnosis according to the divided intervals of this task to indicate which joint suffering from problem accordingly, as indicated in Table II.

### C. Speed Effect on Consumption Profile

To easily show the effect of speed on a power consumption profile of the considered robot manipulator, experimental measurements have been conducted under two different speeds of a particular task, and accordingly, the power patterns are shown in Fig. 19.

As indicated in the figure, a significant difference of consumption patterns of the manipulator between Task 1 that shows the power profile when it took 8 s to end the task, and the same Task 1 when it took 4 s to end the same task. Therefore, the speed of a task is considered in the proposed FDI when initializing the algorithm and creating the reference information.

Since the power pattern of robot consumption is different for different joints faults, interval-based classification of energy residuals is presented to separate the robot faults. Since a particular fault may result in other interval residuals to change, fault isolation is hard only by comparing the patterns of power con-

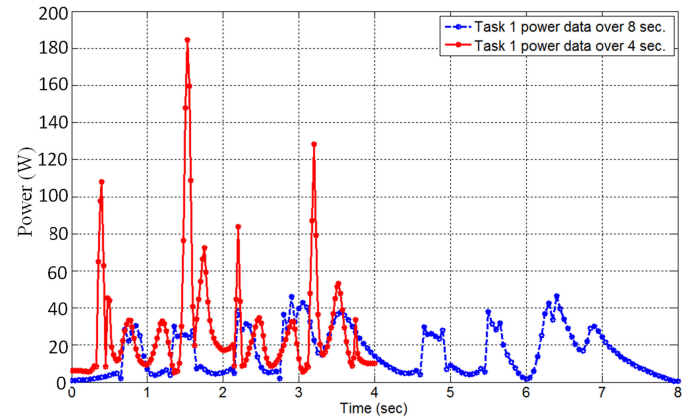


Fig. 19. Power profile of the same task on different speed.

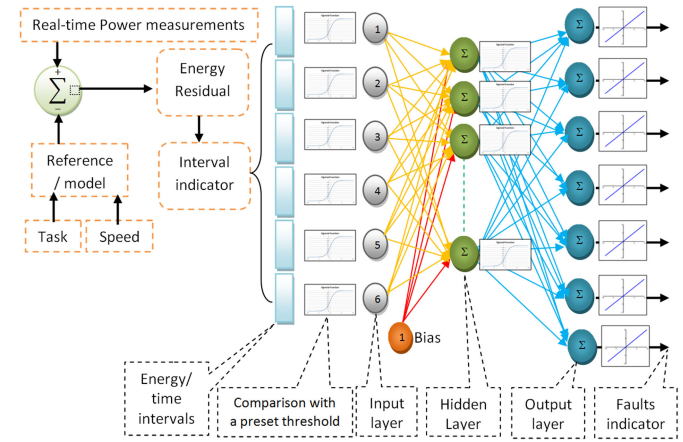


Fig. 20. Faults isolation by ANN.

sumption. To simplify the faults isolation, the artificial neural network (ANN) as a classifier is employed.

### D. ANN-Based Fault Isolation

ANN-based fault detection approach of robot manipulators was considered in [2], [3], [30], and [31]. However, the fault detection methods depend on a user-defined restriction over the modeling uncertainty. ANN is one of the methods that have the ability to do the mapping from fault indications to fault isolation. Feed-forward back-propagation network that is an ANN architecture consisting of an input layer, output layer, and the single hidden layer is adopted here. The faults isolation algorithm by ANN is shown in Fig. 20.

In this strategy, the iteration process of training the network is performed only one time per each task including the speed on healthy measurements, so that later the fault isolation stage is fast. The neural network is configured so that the input neurons are equal to the number of created intervals ( $i_n$ ), suggested three times that number for hidden neurons, and  $(6+1)$  neurons for output layer that is equivalent to the number of robot joints. The training samples are set to be ( $\text{input} \in \mathbb{R}^{i_n * 6}$ ).

**TABLE III**  
FAULT ISOLATION RESULT OF PICK-AND-PLACE TASK

Fault	Output code	Network outputs						
		Y1	Y2	Y3	Y4	Y5	Y6	Y7
1	100000	0.98	0.00	0.00	0.00	0.00	0.00	0.00
	0	7	4	0	5	4	1	3
2	010000	0.00	0.97	0.00	0.00	0.00	0.00	0.00
	0	0	2	0	5	6	7	5
3	001000	0.00	0.00	0.98	0.00	0.00	0.00	0.00
	0	4	4	4	4	4	4	4
4	000100	0.00	0.00	0.00	0.99	0.00	0.00	0.00
	0	3	4	0	4	4	4	4
5	000010	0.00	0.00	0.00	0.00	0.96	0.01	0.99
	1	3	4	4	4	7	1	5
6	000001	0.00	0.00	0.00	0.00	0.00	0.95	0.00
	0	8	4	4	4	9	0	0
free	000010	0.00	0.00	0.00	0.00	0.95	0.00	0.99
	1	5	2	2	2	4	0	7

According to the interval indicator of the robot software driver, the energy residual vector is compared with a preset threshold ( $\varepsilon_j = \pm 10\%$  over the reference/model values) to allow the consideration of some tolerance and noise effect. Therefore, the input layer of the neural network receives logical values given by

$$(\text{input} \in \mathbb{R}^{i_n * 6}) = \begin{cases} 0 & \text{for } |r_j| \leq \varepsilon_j \\ 1 & \text{for } r_j > \varepsilon_j \quad (j = 1, 2, \dots, 6) \\ -1 & \text{for } r_j < \varepsilon_j \end{cases} \quad (20)$$

The columns in **Table I** represent the training input samples, while the last row represents the corresponding target vector. The contents of **Table I** are set as input vectors and desired outputs to the network. After the training is finished, the result of the network can be listed in **Table III**.

The criteria to indicate the fault is the maximum number for each output vector. It is clear that the isolation of each fault is very accurate.

## VI. CONCLUSION

This article presented a data-driven FDI for diagnosing the faulty robot joints by monitoring the energy consumption rate. It utilized the BEVF to obtain historical healthy reference and generate the power patterns. Then, an ANN was presented to generate isolation indicators. According to the above results and discussion, some conclusions can be listed as follows.

- 1) The proposed strategy was successful in detecting and isolating single and multifaults of the considered manipulator although it utilized only the user encoders connector and the measure on the main power supply line.
- 2) An automatic and integrated strategy for FDI was easy to implement based on initializing the algorithm by recording the fault-free measurements of both encoders and power consumption of a robot manipulator for a particular task and speed.
- 3) BEVF, as a robust algorithm to modeling measurements with sharp variations and many resonance peaks, could be used to estimate the power consumption pro-

files of a robot manipulator. Modeling complexity increases with the existence of sharp changes in the power measurements.

- 4) The detection of faults was performed by comparing the relative changes of references for joints positions (encoders) and consumption pattern with the corresponding real-time measurements, while the fault isolation was performed by a neural network that designed and trained initially on a healthy data.
- 5) This approach can help in modeling, monitoring, and fault diagnosing of a wide range of robotic systems.

Redefining for detection thresholds need to be considered in future work as a dynamic change per each task as a function of operation time. The proposed approach requires a new initialization per each task or change in its conditions since the power profile has changed.

## REFERENCES

- [1] A. C. Bittencourt, K. Saarinen, S. Sander-Tavallaey, S. Gunnarsson, and M. Norrlöf, "A data-driven approach to diagnostics of repetitive processes in the distribution domain—Applications to gearbox diagnostics in industrial robots and rotating machines," *Mechatronics*, vol. 24, pp. 1032–1041, 2014.
- [2] X. Q. Liu, H. Y. Zhang, J. Liu, and J. Yang, "Fault detection and diagnosis of permanent-magnet DC motor based on parameter estimation and neural network," *IEEE Trans. Ind. Electron.*, vol. 47, no. 5, pp. 1021–1030, Oct. 2000.
- [3] I. Eski, S. Erkaya, S. Savas, and S. Yildirim, "Fault detection on robot manipulators using artificial neural networks," *Robot. Comput. Integr. Manuf.*, vol. 27, pp. 115–123, 2011.
- [4] R. Aguilar-López and R. Martínez-Guerra, "Robust state estimation for repetitive operating mode process: Application to sequencing batch reactors," *Chem. Eng. J.*, vol. 126, pp. 155–161, 2007.
- [5] W. E. Dixon, I. D. Walker, D. M. Dawson, and J. P. Hartranft, "Fault detection for robot manipulators with parametric uncertainty: A prediction-error-based approach," *IEEE Trans. Robot. Autom.*, vol. 16, no. 6, pp. 689–699, Dec. 2000.
- [6] D. Meike and L. Ribickis, "Energy efficient use of robotics in the automobile industry," in *Proc. 15th Int. Conf. Adv. Robot.*, 2011, pp. 507–511.
- [7] A. Liu, H. Liu, B. Yao, W. Xu, and M. Yang, "Energy consumption modeling of industrial robot based on simulated power data and parameter identification," *Adv. Mech. Eng.*, vol. 10, pp. 1–11, 2018.
- [8] A. Mohammed, B. Schmidt, and L. Wang, "Energy-efficient robot configuration for assembly," *J. Manuf. Sci. Eng.*, vol. 139, pp. 1087–1357, 2017.
- [9] A. Rassölkkin, H. Höimoja, and R. Teemets, "Energy saving possibilities in the industrial robot IRB 1600 control," in *Proc. 7th Int. Conf. Workshop Compat. Power Electron.*, 2011, pp. 226–229.
- [10] D. Meike, M. Pellicciari, and G. Berselli, "Energy efficient use of multi-robot production lines in the automotive industry: Detailed system modeling and optimization," *IEEE Trans. Autom. Sci. Eng.*, vol. 11, no. 3, pp. 798–809, Jul. 2014.
- [11] M. Pellicciari, G. Berselli, F. Leali, and A. Vergnano, "A method for reducing the energy consumption of pick-and-place industrial robots," *Mechatronics*, vol. 23, pp. 326–334, 2013.
- [12] Paryanto, M. Brossog, J. Kohl, J. Merhof, S. Spreng, and J. Franke, "Energy consumption and dynamic behavior analysis of a six-axis industrial robot in an assembly system," *Procedia CIRP*, vol. 23, pp. 131–136, 2014.
- [13] Paryanto, M. Brossog, M. Bornschlegl, and J. Franke, "Reducing the energy consumption of industrial robots in manufacturing systems," *Int. J. Adv. Manuf. Technol.*, vol. 78, pp. 1315–1328, 2015.
- [14] M. Lutovac Banduka, "Remote monitoring and control of industrial robot based on android device and Wi-Fi communication," *Automatika—J. Control Meas. Electron. Comput. Commun.*, vol. 56, pp. 281–291, 2015.
- [15] J. Wu, J. Wang, and Z. You, "An overview of dynamic parameter identification of robots," *Robot. Comput.-Integr. Manuf.*, vol. 26, pp. 414–419, 2010.

- [16] M. M. Olsen, J. Swevers, and W. Verdonck, "Maximum likelihood identification of a dynamic robot model: Implementation issues," *Int. J. Robot. Res.*, vol. 21, pp. 89–96, 2002.
- [17] L. Sciavicco, B. Siciliano, and L. Villani, "Lagrange and Newton-Euler dynamic modeling of a gear-driven robot manipulator with inclusion of motor inertia effects," *Adv. Robot.*, vol. 10, pp. 317–334, 1995.
- [18] A. Calanca, L. M. Capisani, A. Ferrara, and L. Magnani, "MIMO closed loop identification of an industrial robot," *IEEE Trans. Control Syst. Technol.*, vol. 19, no. 5, pp. 1214–1224, Sep. 2011.
- [19] A. Janot, P. Olivier Vandajon, and M. Gautier, "An instrumental variable approach for rigid industrial robots identification," *Control Eng. Pract.*, vol. 25, pp. 85–101, 2014.
- [20] K. Paes, W. Dewulf, K. Vander Elst, K. Kellens, and P. Slaets, "Energy efficient trajectories for an industrial ABB robot," *Procedia CIRP*, vol. 15, pp. 105–110, 2014.
- [21] L. Wang, A. Mohammed, X. V. Wang, and B. Schmidt, "Energy-efficient robot applications towards sustainable manufacturing," *Int. J. Comput. Integr. Manuf.*, vol. 31, pp. 692–700, 2018.
- [22] M. Pettersson, *Design Optimization in Industrial Robotics Methods and Algorithms for Drive Train Design*, no. 1170, 2008.
- [23] A. H. Sabry, W. Z. W. Hasan, M. Z. A. Ab Kadir, M. A. M. Radzi, and S. Shafie, "DC-based smart PV-powered home energy management system based on voltage matching and RF module," *PLoS One*, vol. 12, no. 9, p. e0185012, 2017.
- [24] A. H. Sabry, W. Z. W. Hasan, M. Z. A. Ab Kadir, M. A. M. Radzi, and S. Shafie, "Field data-based mathematical modeling by Bode equations and vector fitting algorithm for renewable energy applications," *PLoS One*, vol. 13, no. 1, p. e0191478, 2018.
- [25] *DC Servo Motor Parameter Estimation—MATLAB & Simulink Example*. [Online]. Available: <https://www.mathworks.com/help/sldc/examples/dc-servo-motor-parameter-estimation.html>. Accessed on: Jun 20, 2017.
- [26] R. Saidur, "A review on electrical motors energy use and energy savings," *Renewable Sustain. Energy Rev.*, vol. 14, no. 3, pp. 877–898, 2010.
- [27] B. Gustavsen and A. Semlyen, "Rational approximation of frequency domain responses by vector fitting," *IEEE Trans. Power Del.*, vol. 14, no. 3, pp. 1052–1059, Jul. 1999.
- [28] A. H. Sabry, W. Z. W. Hasan, M. Z. A. Ab Kadir, M. A. M. Radzi, and S. Shafie, "Field data-based mathematical modeling by Bode equations and vector fitting algorithm for renewable energy applications," *PLoS One*, vol. 13, no. 1, Jan. 2018, Art. no. e0191478.
- [29] *Curve Fitting Toolbox—MATLAB*. MATLAB. [Online]. Available: <https://www.mathworks.com/products/curvefitting.html>. Accessed on: May 6, 2019.
- [30] A. T. Vemuri and M. M. Polycarpou, "Neural-network-based robust fault diagnosis in robotic systems," *IEEE Trans. Neural Netw.*, vol. 8, no. 6, pp. 1410–1420, Nov. 1997.
- [31] W. E. Dixon, I. D. Walker, D. M. Dawson, and J. P. Hartranft, "Fault detection for robot manipulators with parametric uncertainty: A prediction-error-based approach," *IEEE Trans. Robot. Autom.*, vol. 16, no. 6, pp. 689–699, Dec. 2000.



**Ahmad H. Sabry** was born in Baghdad, Iraq. He received the B.Sc. and M.Sc. degrees in electrical and electronics, control and automation, engineering from the University of Technology, Baghdad, in 1994 and 2001, respectively, and the Ph.D. degree in dc-based photovoltaic-powered home energy system from the Department of Electrical and Electronic Engineering, Control and Automation, Universiti Putra Malaysia, Selangor, Malaysia, in 2017.

He is currently a Postdoctoral Researcher with Universiti Tenaga Nasional, Selangor. He is the author of more than 35 articles, and more than five inventions, and holds one patent. His research interests include integrated solar powered smart home system based on voltage matching, dc distribution, industrial robotic systems, and wireless energy management systems.

Dr. Sabry is a Reviewer in more than three ISI journals.



**Farah Hani Nordin** received the bachelor's (Hons.) degree in electrical and electronic engineering from Universiti Tenaga Nasional (UNITEN), Selangor, Malaysia, in 2000, the M.Sc. degree in control, communication and digital signal processing from the University of Strathclyde, Glasgow, U.K., in 2002, and the Ph.D. degree in engineering from UNITEN in 2010.

She is an Associate Professor and currently holding the position of Deputy Dean (student affairs and external relations) with the College of Engineering, UNITEN, where she has previously served as the Head of the Department of Electronics and Communication Engineering from 2014 until 2018.

Dr. Nordin is a member of The Institution of Engineers Malaysia and also registered as a Professional Engineer under the Board of Engineers Malaysia.



**Ameer H. Sabry** received the B.Sc. degree in mechanical engineering from Al-Mustansirya University, Baghdad, Iraq, in 2003, the M.Sc. degree in mechanical and aeronautical engineering from the University of Turkish Aeronautical Association, Ankara, Turkey, in 2017, and is currently working toward the Ph.D. degree in industrial robot with the Institute of Power Engineering, University Tenaga National, Selangor, Malaysia.

He is currently with the Ministry of Electricity, Baghdad. His research interests include fault detection and diagnosis, industrial robot, and renewable energy and its applications.



**Mohd Zainal Abidin Ab Kadir** (M'06) received the B.Eng. degree in electrical and electronic engineering from the Universiti Putra Malaysia, Selangor, Malaysia, in 2001, and the Ph.D. degree in high-voltage engineering from the University of Manchester, Manchester, U.K., in 2006.

He is currently a Strategic Hire Professor with the Institute of Power Engineering, Universiti Tenaga Nasional, Selangor, and a Professor with the Faculty of Engineering, Universiti Putra Malaysia. He is the Founding Director with the

Centre for Electromagnetic and Lightning Protection Research, Universiti Putra Malaysia. To date, he has authored and coauthored more than 300 journals and conference papers. His research interests include high-voltage engineering, lightning protection, electromagnetic compatibility, and power system transients.

Dr. Abidin Ab Kadir is also an IEEE Power and Energy Society Distinguished Lecturer in the field of lightning and high-voltage engineering.